Pacific Graphics 2013
B. Levy, X. Tong, and K. Yin
(Guest Editors)

Volume 32 (2013), Number 7

Symmetry Robust Descriptor for Non-Rigid Surface Matching

Zhiyuan Zhang† KangKang Yin‡ Kelvin W.C. Foong§

National University of Singapore, Singapore

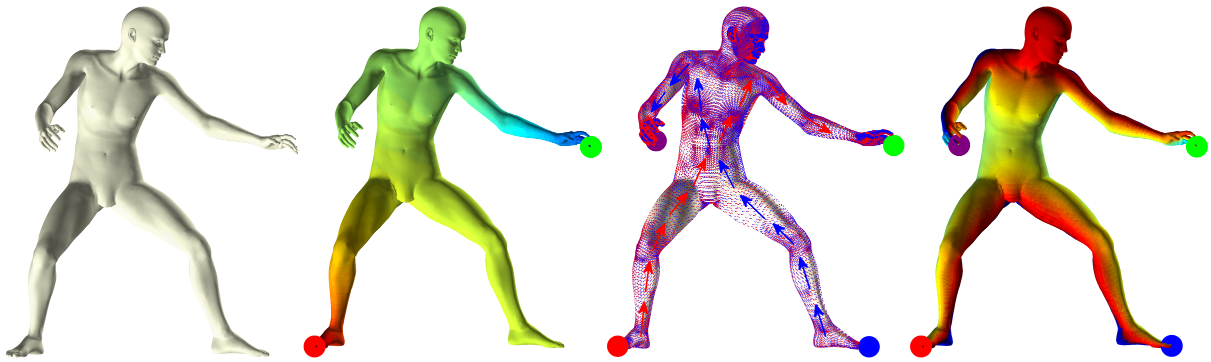

Figure 1: *Signed angle field computation: (a) a human model; (b) the harmonic field from the red point on the right foot to the green point on the left hand; (c) the two gradient fields of the harmonic fields derived from four points on the hands and feet; (d) the signed angle field ranging from $-\pi$ to π and visualized from blue to red.*

Abstract

In this paper, we propose a novel shape descriptor that is robust in differentiating intrinsic symmetric points on geometric surfaces. Our motivation is that even the state-of-the-art shape descriptors and non-rigid surface matching algorithms suffer from symmetry flips. They cannot differentiate surface points that are symmetric or near symmetric. Hence a left hand of one human model may be matched to a right hand of another. Our Symmetry Robust Descriptor (SRD) is based on a signed angle field, which can be calculated from the gradient fields of the harmonic fields of two point pairs. Experiments show that the proposed shape descriptor SRD results in much less symmetry flips compared to alternative methods. We further incorporate SRD into a stand-alone algorithm to minimize symmetry flips in finding sparse shape correspondences. SRD can also be used to augment other modern non-rigid shape matching algorithms with ease to alleviate symmetry confusions.

1. Introduction

Non-rigid surface matching is the foundation of many shape analysis and retrieval applications [TV08, vKZHCO11]. While recent years have seen many advances on both sparse and dense shape matching [KLF11, SY13], most existing algorithms are easily confused by intrinsically symmetric features and suffer from *symmetry flips*. For example, methods based on geodesic distances or geometric quantities alone are commonly confused by symmetries present in humans and animals. Thus points on a left hand of one model may be matched to points on a right hand of another. This is because

† cszyzhang@gmail.com
‡ kkyin@comp.nus.edu.sg
§ kelvinfoong@nuhs.edu.sg

geometric information mainly concerns about distances that cannot differentiate symmetric or near symmetric features.

Our intuition is to incorporate surface orientation in differentiating symmetric features. Given two pairs of feature points, we construct two harmonic fields and their gradient fields respectively. We then intersect these gradient fields to derive a *signed angle field* that introduces a sense of orientation and thus is capable of discriminating mirror symmetry. We will detail the signed angle field computation in Section 3. In Section 4, we further construct a Symmetry Robust Descriptor (SRD) using two signed angle fields generated from different orderings of the same four-point tuples. We also show how to incorporate SRD into a sparse matching algorithm to alleviate symmetry flips in Section 5. We conduct two experiments to validate the effectiveness of our shape descriptor and matching algorithm in Section 6. Finally, we conclude our work with a detailed discussion of its limitations.

In summary, our contributions are: (a) we propose a novel shape descriptor SRD based on signed angle fields that can robustly differentiate two pairs of points, even when they are symmetric or near symmetric; (b) we demonstrate that SRD can be integrated into existing non-rigid surface matching algorithms with ease.

2. Related Work

Non-rigid shape matching is a target of extensive research. Due to space limit, we only discuss prior work most relevant to our own and refer interested readers to survey papers [TV08, vKZHCO11] for more complete views of the field.

Multi-Dimensional Scaling (MDS) transforms geodesic distances into Euclidean distances and thus translates the problem of matching deformable objects into a simpler problem of matching rigid objects [EK03]. Certain Eigenmodes can be switched under shape stretching, which is handled with non-rigid ICP (Iterative Closest Point) alignment based on thin-plate splines in [JZ06]. Generalized Multi-Dimensional Scaling (GMDS) improves MDS by finding the least distortion embedding of one surface into another directly [BBK06]. More recently [SY12] rely on MDS to find the initial correspondences and then refine the results by an EM (Expectation-Maximization) procedure. MDS-based spectral correspondence techniques, however, generally suffer from the sign flipping problem in eigenvector computation which results in symmetry flips. We will show how to incorporate our descriptor to handle this problem.

Sun et al. [SCF10] propose a descriptor based on fuzzy geodesics for finding sparse correspondences for deformable shapes. Although more consistent than previous methods based on normal geodesic distances, it still suffers from symmetry flips. We will compare our SRD to their descriptor. The strength of our descriptor is that it takes into account the surface orientation.

Recently, descriptors based on pairwise feature points have been adopted more and more in shape matching. 4-Points congruent sets support robust rigid surface registration [AMCO08]. Zheng et al. [ZTZX12] propose iso-lines of harmonic fields between pairs of interest points as a descriptor for shape analysis. In [vKZH13] another pairwise descriptor aggregates areas of the faces along the path from one point to the other into different bins. Our SRD is partially inspired by these pairwise descriptors.

Most recently twisting symmetry flips can be reduced by penalizing transformations that deviate too much from a pure rotation [ATCO*10] or large deformation distortions [ZSCO*08]. Global reflective symmetry axis curves are found to be robust for shape correspondences [LKF12]. The work of [OMPG13] is designed to address the symmetric ambiguity problem present when matching shapes with intrinsic symmetries, and thus shares the same goal as ours. Their method performs shape matching in a quotient space of the functional space [OBCS*12] where the symmetry has been identified and factored out [LCDF10]. It needs one reference shape with known symmetry for each category of models in advance, and cannot handle models with severe deformation.

3. Signed Angle Field

Our novel shape descriptor is based on a scalar field that we call signed angle field. A signed angle field builds upon two gradient fields, which are vector fields computed from harmonic fields. We now detail the construction of these fields.

3.1. Harmonic Field

Given two points we first construct a harmonic field that is a scalar function f defined for each vertex of a surface that satisfies $\Delta f = 0$, where Δ is the Laplace-Beltrami operator, subject to certain Dirichlet boundary constraints. On a triangle mesh surface, Δ can be discretized as

$$\Delta_i = \sum_{j \in N_i} w_{ij}(u_j - u_i)$$

where N_i indicates the neighboring vertices of i. w_{ij} is the weight of edge (i, j), and we use the contangent scheme [MDSB03]:

$$w_{ij} = -\frac{1}{2}(cot\alpha_{ij} + cot\beta_{ij})$$

where α_{ij} and β_{ij} are the angles facing the edge in the two faces sharing the edge. Rewrite the Laplacian operator equation as a matrix, we get

$$\Delta f = -Lf$$

where L is a sparse N by N matrix with entries:

$$L_{ij} = \begin{cases} \sum_j w_{ij}, & \text{if } i = j \\ -w_{ij}, & \text{if } j \in N_i \\ 0, & \text{otherwise} \end{cases}$$

For any point pair (p,q), a harmonic field can be constructed by solving the sparse linear system $Lf = 0$ with constraints $f(p) = 0$ and $f(q) = 1$. We refer interested readers to [MDSB03, SCOL*04, DKG05] for more details.

Harmonic fields offer many desired properties: they are smooth; their local extremes coincide with singularities; and they are invariant to isometric deformations due to the use of cotangent weights that reduces the sensitivity to noise and tessellation. Figure 1(b) shows an example of the harmonic field from a point on the right foot (red) to a point on the left hand (green). The field varies smoothly between these two points as indicated by the color distribution.

3.2. Gradient Field

Once we compute the harmonic field between two points p and q, its gradient field can be derived straightforwardly. For any face (i, j, k) in the triangle mesh we solve

$$\begin{bmatrix} x_j - x_i \\ x_k - x_j \\ n \end{bmatrix} \begin{bmatrix} g \end{bmatrix} = \begin{bmatrix} u_j - u_i \\ u_k - u_j \\ 0 \end{bmatrix} \quad (1)$$

where $x_i, x_j, x_k \in \Re^3$ are the vertices of the face, and u_i, u_j, u_k are the scalar values from the harmonic field for these vertices. Since the gradient field is derived from the harmonic field, it possesses the same nice properties such as smoothness, isometric invariance and insensitivity to noise. In Figure 1(c), we show the gradient fields constructed from two harmonic fields: one is from the right foot to the left hand and the other is from the left foot to the right hand.

3.3. Signed Angle Field

Given two normalized gradient fields G_a and G_b, we can construct a signed angle field through their intersection as follows. On face i of a triangle mesh, we calculate the included angle between the two gradient vectors (G_{a_i}, G_{b_i}). To determine its sign, we check the directions of the face normal n_i and the two gradient vectors. Thus the signed angle A_i for face i is

$$A_i = D \cdot acos(dot(G_{a_i}, G_{b_i})) \quad (2)$$

where D is the sign indicator determined by

$$D = \begin{cases} +1, & \text{if } dot(cross(G_{a_i}, G_{b_i}), n_i) > 0 \\ -1, & \text{otherwise} \end{cases} \quad (3)$$

The above signed angle field mainly has two advantages when applied to non-rigid surface matching for shapes with global intrinsic symmetry. First, it inherits the nice properties of harmonic fields: smoothness, isometric invariance, and insensitivity to noise. In Figure 2, we show two examples of signed angle fields. The shapes in the first row are near-isometric while the shapes in the second row are not. The signed angle fields for both cases, however, are similar. This is essential for non-rigid shape matching.

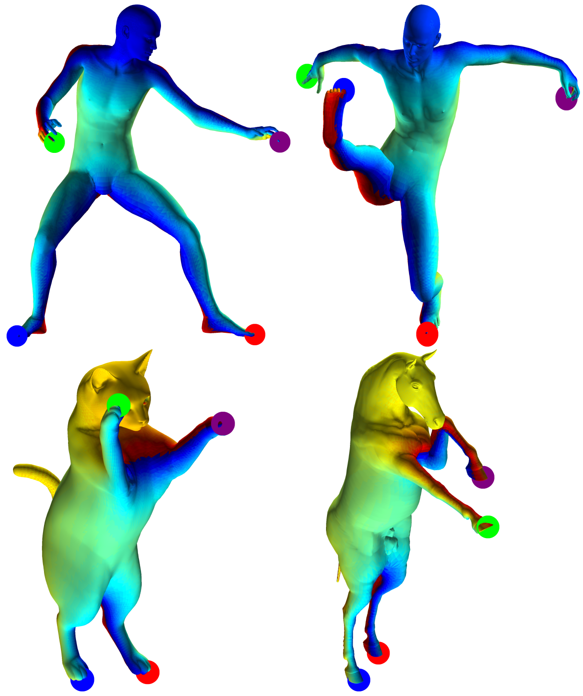

Figure 2: *Similarity between signed angle fields for near-isometric(top) and non-isometric(bottom) shapes.*

The second strength of the signed angle field is its ability to differentiate symmetric features. Existing shape matching algorithms usually check the compatibility of geodesic distances or geometric descriptors between interest points. Thus they cannot tell the correct matches from their symmetrically flipped ones. For example, when matching the first shape in Figure 2 to itself, the left limbs are easily mismatched to the right limbs by pure geometry based descriptors. In contrast, our proposed signed angle field takes into account surface directions, e.g., flow from left to right or from right to left, and thus can differentiate symmetric points. As we can see, the signed angle field on top left of Figure 2 is different from the field of Figure 1(d), even though the point pairs are symmetric.

4. Symmetry Robust Descriptor

We now propose a novel shape descriptor based on the signed angle fields introduced above. Given four points [rf (right foot), lh (left hand), lf (left foot), rh (right hand)] on a surface as shown in Figure 3(a), we first construct a signed angle field $A_{[(rf,lh),(lf,rh)]}$ from the two gradient fields

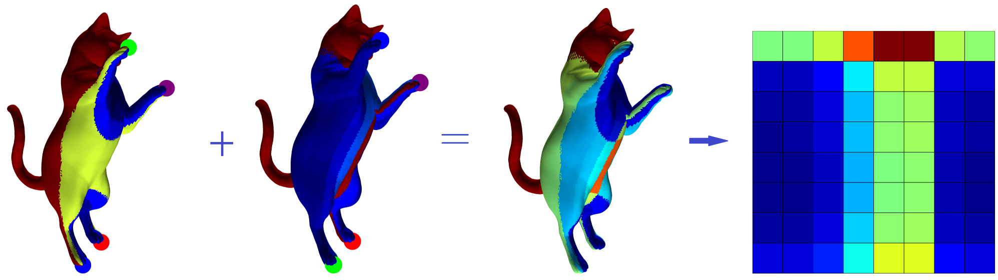

(a) (b) (c) (d)

Figure 4: *SRD construction: given four points [lf, rh, rf, lh], we can construct two signed angle fields – (a) from [(lf,rh),(rf,lh)], and (b) from [(lf,rf),(rh,lh)]. For each signed angle field we can build one 1D descriptor by allocating the faces into bins according to their signed angle values uniformly divided in the range* $(-\pi, +\pi)$*, and then accumulating the areas of the faces that belong to a particular bin. We use different colors to visualize bin values in the figure. Then the two 1D descriptors are combined into a 2D descriptor as shown in (d).*

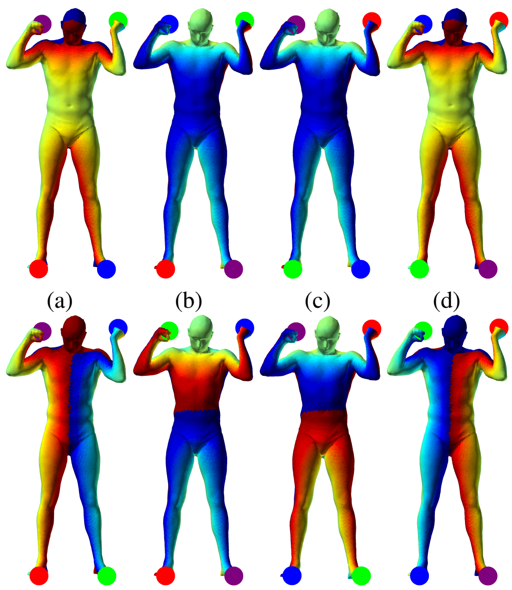

(a) (b) (c) (d)

(e) (f) (g) (h)

Figure 3: *Eight signed angle fields from different permutations of the same four-point tuple. We always compute the signed angle fields from the points in the order of [(red,green),(blue,purple)].*

$G_{(rf,lh)}$ and $G_{(lf,rh)}$ as described in the last section. A one dimensional descriptor can then be built by allocating the faces into k bins according to their signed angle values uniformly divided in the range $(-\pi, +\pi)$. Then we accumulate the areas of all the faces that belong to a particular bin as the bin value.

Next we compute the signed angle field $A_{[(rf,lf),(lh,rh)]}$ from gradient fields $G_{(rf,lf)}$ and $G_{(lh,rh)}$ (Figure 3(e)). This switching of the second and third points gives another 1D descriptor. By combining the above two 1D descriptors from the two angle fields formed by the same set of four points, although in different orders, we obtain a 2D shape descriptor of size k by k. Figure 4 illustrates this process in more details, where the x axis denotes the bin values from the first angle field while y axis denotes the bin values from the second angle field. This descriptor, which we call Symmetry Robust Descriptor (SRD), is able to differentiate symmetric points on surfaces undergone non-rigid deformations, as we will show later.

Note that one single signed angle field alone can be ambiguous in the sense that Figures 3(a) and (d) look exactly the same. This ambiguity of signed angle fields motivates our two dimensional descriptors computed from two signed angle fields, as shown in Figure 4. Similarly, Figures 3(a) and (e) combined is different from Figures 3(d) and (h) combined. For ease of interpretation, we always visualize the two point pairs used for signed angle field computation in [(red, green),(blue,purple)] in all our figures.

5. Sparse Shape Correspondence

In this section, we incorporate SRD into the algorithm of [JZ06] to minimize symmetry flips in finding correspondences between two sets of sparse interest points on two given shapes.

We first compute Heat Kernel Signature (HKS) for all the surface points and sort the values at a large instant ($t = 100$) in descending order [SOG09]. We then iteratively select a set of sparse points that roughly cover the whole surface evenly. More specifically, we select the point with the largest HKS as the first sparse point, and mark its neighbors within a radius r as covered. Then from all the remaining uncovered points, we select the point with the largest HKS and again mark its neighbors within a radius r as covered. We iterate this process until all the surface points are covered. For our tested models and a properly set r, about 100 sparse points are selected this way. Among all the chosen sparse points, we detect the local maxima as *extreme points*, and use their SRDs for symmetry differentiation. These extreme points are more stable and consistent than the rest of the sparse points, and usually about $5 \sim 10$ extreme points exist in our tested models.

Next we utilize the method of [JZ06] to embed all the sparse points into a six dimensional spectral domain. More specifically, we first calculate the pairwise geodesic distances between all pairs of sparse points, and construct an affinity matrix whose entries are the pairwise geodesic distances smoothed by a Gaussian kernel. We then compute the eigenvectors of the affinity matrix, and embed all the sparse points into the spectral domain formed by the six non-constant leading eigenvectors. The sparse points of the two shapes are then matched based on the L_2 distance of their spectral embedding coordinates. We refer interested readers to [JZ06] for more details of the embedding method.

Due to arbitrary sign flips of eigenvectors, however, there are 2^k possible ways for the embeddings. The embeddings that minimize the summed distances of all matched sparse points are selected in [JZ06]. Such embeddings, however, can suffer from symmetry flips. We thus compute the SRD distances from the extreme points, and choose the embeddings that minimize the summed SRD distances. Note that we do not need to compute the SRD for every 4-point combination of the extreme points. Suppose there are n extreme points on the source shape, we find it sufficient to just compute n SRDs from tuples $[(1,2),(3,4)],[(2,3),(4,5)],...,[(n-1,n),(1,2)],[(n,1),(2,3)]$. After the correct embeddings are identified by SRDs from the extreme points, the rest of the sparse points can then be easily matched to their nearest neighbors in the chosen spectral embeddings.

6. Results

To show the effectiveness of the proposed descriptor, we conduct two experiments: a permutation test and a shape matching comparison. The permutation experiment is to testify SRD's ability to identify the ground truth from permutations with symmetry flips; the shape matching test compares our SRD-based algorithm with several state-of-the art algorithms by finding sparse correspondences between two input meshes. For both experiments, we use 2D SRD descriptors of size 6 by 6.

6.1. Data set

We use a subset of watertight models from the SHREC2007 Benchmark [GBP07] which contains 400 meshes in 20 object categories. We select three categories of objects: human, hand, and Armadillo, which contain 18, 20, and 20 models, respectively. We use the manual labeling provided by [KLF11] as the ground truth. We do not use models such as octopus in the dataset because they are highly symmetric shapes with multiple solutions.

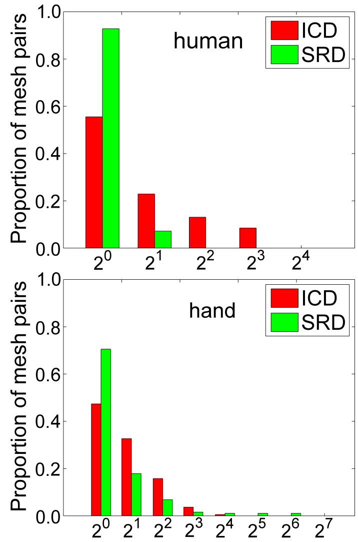

Figure 5: *Statistics of the permutation test on when the ground truth appears.*

6.2. Permutation test

We conduct a permutation test similar to that of [SCF10], which uses a 4-point based method for non-rigid shape matching as well. They compute the Intersection Configuration Distance (ICD) between two pairs of 4-point tuples, and showed that ICD is more powerful than GDD (the differences of pairwise geodesic distances). We thus only compare the performance of SRD to that of ICD.

We use the human and hand models for comparison with ICD. For each pair of meshes to be matched, we generate all possible permutations of their extreme points. We then compute and rank the matching error for each permutation. Similar to [SCF10], we check the sorted list and record the first position when the ground truth appears. The earlier the ground truth appears, the better the algorithm is in terms of avoiding symmetry flips.

The statistics of our test is shown in Figure 5. For both datasets, SRD outperforms ICD. The ground truth is found as the best match for more than 90% and 70% for humans and hands, respectively, among all the mesh pairs using SRD. The improvement over ICD, more than 30% and 20% respectively, is significant. Note that this plot is different from those of [SCF10] where ICD achieved nearly 100% for these datasets. This is because [SCF10] treats the symmetrically flipped matchings as correct matching. In our experiments, however, we only accept the ground truth without symmetry flips as correct, so that the matching should not

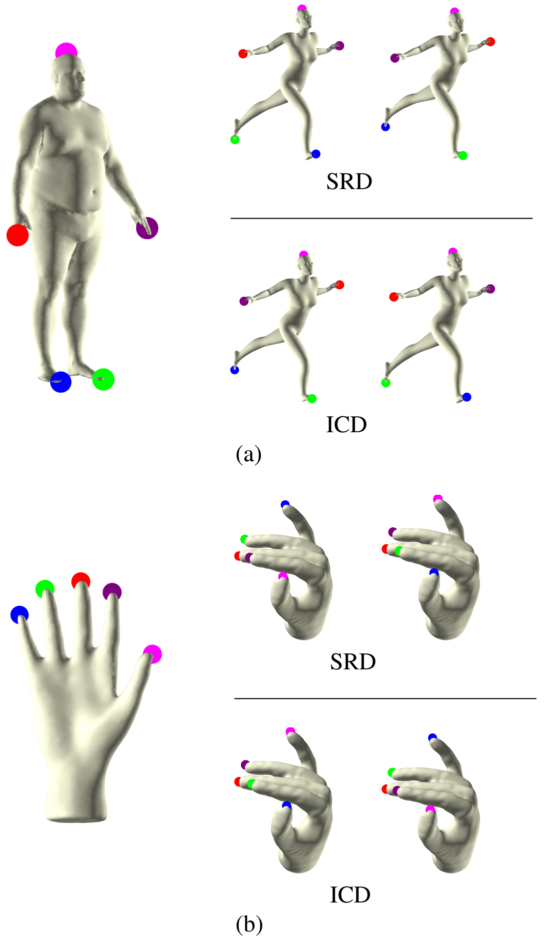

Figure 6: *Top two matches for human and hand shape correspondence: the first row in each subfigure is the result of SRD while the second row is the result of ICD. Corresponding points are colored the same. As we can see, SRD usually finds the correct permutation as the best match; while ICD returns more symmetrically flipped permutations as the best match, even though it can return the ground truth as one of the top matches.*

confuse the left and right sides of a human. In Figure 6, we show examples of matching a man to a woman, and matching a neutral hand to a deformed hand. The first two best matches are shown on the right side. We see that SRD usually ranks the ground truth higher than ICD.

Note that SRD does not perform as well for the hand models as for the human models, mainly because there are both right hands and left hands in the hand dataset. In this case, SRD will not rank the manually labeled "ground truth" (left thumb to right thumb etc.) high up in the returned list. We treat this as a desirable feature as there are cases where we just need to retrieve left hands from an input model of a left hand. Still SRD outperforms ICD, which can be easily confused by symmetry or quasi-symmetry, such as the last row

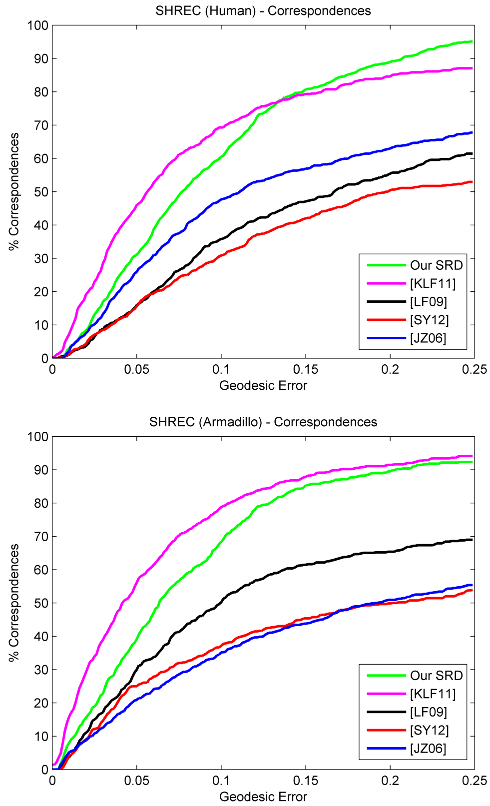

Figure 7: *Comparison of our SRD-based shape matching with four state-of-the-art methods.*

in Figure 6 where the best permutation matched the thumb to the pinky.

6.3. Finding Sparse Correspondences

We evaluate the matching scheme described in Section 5 using the protocol of [KLF11]. We use the Human and Armadillo datasets, which contain both symmetric and severely deformed shapes. We compare our method with four latest shape matching algorithms [JZ06], [LF09], [KLF11], and [SY12]. The results are shown in Figure 7.

Our method outperforms the sparse matching algorithms but is slightly worse than the BIM (Blended Intrinsic Maps) method of [KLF11]. As our method is designed for sparse matching only, we believe its performance can be further improved if appropriate mechanism is added to extend our sparse matching into dense matching. We also show some matching examples in Figure 8, where matched point pairs are colored the same and symmetry flips are connected by lines. We can see that both [LF09] and [SY12] have symmetry flips, which are avoided with our method.

The performance statistics of our SRD-based shape

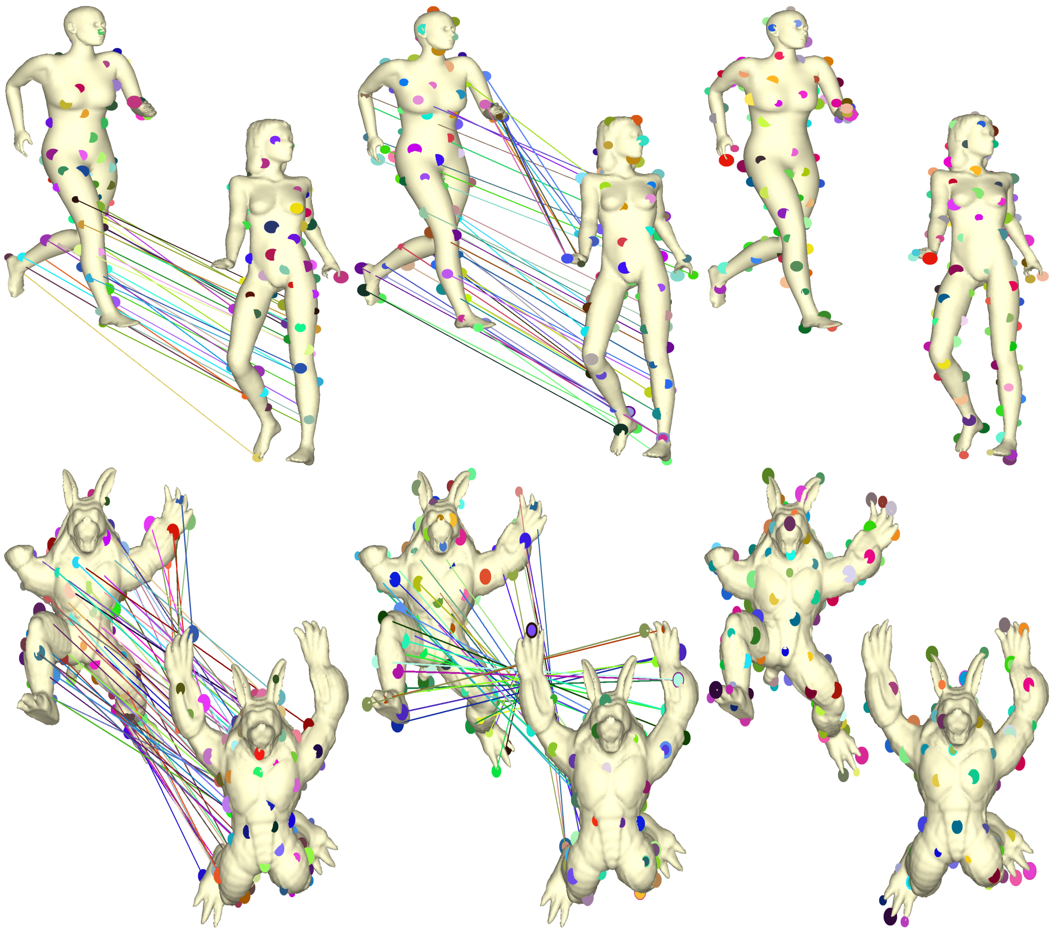

Figure 8: *Comparison of three methods: (a) [LF09] (b) [SY12] (c) ours. Matched point pairs are colored the same. Symmetry flips are connected by lines.*

matching is listed in Table 1. Our code is in Matlab and unoptimized. Timing was measured in seconds on a laptop with Pentium Dual-Core CPU T4300, 2.10GHz and 4G RAM. For example, for a human model of 11015 vertices, we extracted 100 sparse points in about 4.2 seconds, among which 5 are extreme points. Harmonic fields computation for all pairs of extreme points took about 1.9 seconds. SRDs computation took about 0.8 seconds. In total, all computations for one human model took about 8.8 seconds. Thus matching two human shapes from scratch takes about 18 seconds. However, for shape retrieval applications, we can pre-compute relevant quantities for shapes in the database and store their SRDs for fast online shape retrieval.

7. Discussion

We have proposed a symmetry robust descriptor which is able to minimize symmetry flips for sparse matching of deformable surfaces. The key to SRD's success is its awareness of the surface orientation between two pairs of interest points. We have also incorporated SRD into a standalone algorithm for finding sparse correspondences between non-rigidly deformed surfaces. Note that SRD can also be used to complement other existing algorithms with ease. Many shape matching methods search for the best mapping between two shapes by minimizing an objective function which usually has similar values for symmetric features. We can thus use SRD in postprocessing to remove false positives within the top matches returned by such symmetry insensitive algorithms.

There are several limitations of our shape descriptor, however. The computation of SRD depends on the accuracy of the gradient fields and signed angle fields. For instance, it is well known that the gradient of harmonic functions may be hard to compute robustly far from the "sources". Therefore increasing the size of the SRD actually degrades its performance. Experimentally we found SRDs of 6×6 or 8×8 work best. Another effect of inaccurate fields is that SRD

Model	#Vertices	#Sparse(Extreme) Points	Sparse Points Detection	Harmonic Fields	SRDs	Total
Human	11015	100 (5)	4.2	1.9	0.8	8.8
Armadillo	21774	102 (7)	9.3	11.8	2.8	26.9

Table 1: *Performance statistics of each major step of our SRD-based shape matching. Timing is measured in seconds.*

may mismatch nearby feature points, such as matching an index finger tip to a middle finger tip, as can be seen from Figure 8(c). Moreover, SRD is good at differentiating global intrinsic symmetries but not local symmetries, such as the center of the palm and the center of the back of the hand. SRD also does not work well for challenging symmetries that are even hard for humans to detect, such as multiple arms of an octopus.

In the future, we plan to apply SRD to dense surface matching, such as the coarse-to-fine shape correspondence method of [SY13]. We would also like to extend SRD to a 3D descriptor where the third dimension indicates the geodesic distance to one of the four points used to construct SRD. We conjecture such 3D SRD might achieve better performance. In addition, we wish to incorporate Regions of Interest, similar to [vKZH13], to adapt our algorithm for partial shape matching. Note that even though our SRD-based matching does not require complete models, as illustrated by the second row of Figure 8, currently the missing part should remain insignificant.

Acknowledgements: We would like to thank the anonymous reviewers for pointing out errors in our initial draft and providing numerous constructive feedback. This work was partially supported by Singapore Ministry of Education Academic Research Fund Tier 2 (MOE2011-T2-2-152).

References

[AMCO08] Aiger D., Mitra N. J., Cohen-Or D.: 4-points congruent sets for robust pairwise surface registration. *ACM Trans. Graph. 27*, 3 (2008), Article 85. 2

[ATCO*10] Au O. K.-C., Tai C.-L., Cohen-Or D., Zheng Y., Fu H.: Electors voting for fast automatic shape correspondence. *Computer Graphics Forum 29*, 2 (2010), 645–654. 2

[BBK06] Bronstein M. M., Bronstein A. M., Kimmel R.: Generalized multidimensional scaling: a framework for isometry-invariant partial surface matching. *Proceedings of the National Academy of Sciences 103*, 5 (2006), 1168–1172. 2

[DKG05] Dong S., Kircher S., Garland M.: Harmonic functions for quadrilateral remeshing of arbitrary manifolds. *Computer Aided Geometric Design - Special issue: Geometry processing 22*, 5 (2005), 392–423. 3

[EK03] Elad A., Kimmel R.: On bending invariant signatures for surfaces. *IEEE Transactions on Pattern Analysis and Machine Intelligence 25*, 10 (2003), 1285–1295. 2

[GBP07] Giorgi D., Biasotti S., Paraboschi L.: *SHREC2007 3D Shape Retrieval Contest.* Tech. Rep. UU-CS-2007-015, Utrecht University, 2007. 5

[JZ06] Jain V., Zhang H.: Robust 3D shape correspondence in the spectral domain. In *SMI'06* (2006), pp. 118–129. 2, 4, 5, 6

[KLF11] Kim V. G., Lipman Y., Funkhouser T.: Blended intrinsic maps. *ACM Trans. Graph. 30*, 4 (2011), Article 79. 1, 5, 6

[LCDF10] Lipman Y., Chen X., Daubechies I., Funkhouser T.: Symmetry factored embedding and distance. *ACM Trans. Graph. 29*, 4 (2010), Article 103. 2

[LF09] Lipman Y., Funkhouser T.: Möbius voting for surface correspondence. *ACM Trans. Graph. 28*, 3 (2009), Article 72. 6, 7

[LKF12] Liu T., Kim V. G., Funkhouser T.: Finding surface correspondences using symmetry axis curves. *Computer Graphics Forum 31*, 5 (2012), 1607–1616. 2

[MDSB03] Meyer M., Desbrun M., Schröer P., Barr A. H.: Discrete differential geometry operators for triangulated 2-manifolds. *Visualization and Mathematics III* (2003), 35–57. 2, 3

[OBCS*12] Ovsjanikovy M., Ben-Chenz M., Solomonz J., Butscherz A., Guibas L.: Functional maps: a flexible representation of maps between shapes. *ACM Trans. Graph. 31*, 4 (2012), Article 30. 2

[OMPG13] Ovsjanikov M., Mérigot Q., Patraucean V., Guibas L.: Shape matching via quotient spaces. *Computer Graphics Forum 32*, 5 (2013). 2

[SCF10] Sun J., Chen X., Funkhouser T. A.: Fuzzy geodesics and consistent sparse correspondences for deformable shapes. *Computer Graphics Forum 29*, 5 (2010), 1535–1544. 2, 5

[SCOL*04] Sorkine O., Cohen-Or D., Lipman Y., Alexa M., Rössl C., Seidel H.-P.: Laplacian surface editing. In *SGP'04* (2004), pp. 175–184. 3

[SOG09] Sun J., Ovsjanikov M., Guibas L. J.: A concise and provably informative multi-scale signature based on heat diffusion. *Comput. Graph. Forum 28*, 5 (2009), 1383–1392. 4

[SY12] Sahillioglu Y., Yemez Y.: Minimum-distortion isometric shape correspondence using EM algorithm. *IEEE Trans. Pattern Anal. Mach. Intell. 34*, 11 (2012), 2203–2215. 2, 6, 7

[SY13] Sahillioglu Y., Yemez Y.: Coarse-to-fine isometric shape correspondence by tracking symmetric flips. *Computer Graphics Forum 32*, 1 (2013), 177–189. 1, 8

[TV08] Tangelder J. W. H., Veltkamp R. C.: A survey of content based 3d shape retrieval methods. *Multimedia Tools and Applications 39*, 3 (2008), 441–471. 1, 2

[vKZH13] van Kaick O., Zhang H., Hamarneh G.: Bilateral maps for partial matching. *Computer Graphics Forum 32* (2013). 2, 8

[vKZHCO11] van Kaick O., Zhang H., Hamarneh G., Cohen-Or D.: A survey on shape correspondence. *Computer Graphics Forum 30*, 6 (2011), 1681–1707. 1, 2

[ZSCO*08] Zhang H., Sheffer A., Cohen-Or D., Zhou Q., van Kaick O., Tagliasacchi A.: Deformation-drive shape correspondence. *Computer Graphics Forum 27*, 5 (2008), 1431–1439. 2

[ZTZX12] Zheng Y., Tai C.-L., Zhang E., Xu P.: Pairwise harmonics for shape analysis. *IEEE Trans Vis Comput Graph 21* (2012). 2